Electronic Supplementary Material (ESI) for Environmental Science: Nano.

Electronic Supplementary Information (ESI)

Effects of Low-Molecular-Weight Organic Acids on the Dissolution of Hydroxyapatite Nanoparticles

Dengjun Wang,[a] Yunsong Xie,[b] Deb P. Jaisi*[a] and Yan Jin*[a]

[a] *Department of Plant and Soil Sciences, University of Delaware, Newark, DE 19716, United States*

[b] *Department of Physics and Astronomy, University of Delaware, Newark, DE 19716, United States*

*Corresponding Authors:

Deb P. Jaisi

E-mail: jaisi@udel.edu

Yan Jin

E-mail: yjin@udel.edu

#First Author

Dengjun Wang

E-mail: wangdengjun1986@gmail.com

Number of Pages: 16

Number of Tables: 2

Number of Figures: 12

Table S1 Fitted parameters of the exponential decay model for the dissolution rate (R) in the batch experiments

LMWOAs	C_0=0.2 g L^{-1} HANPs			C_0=1 g L^{-1} HANPs		
	d_1	d_2	R^2	d_1	d_2	R^2
Acetic acid	−0.412	−4.13	1.0	−0.340	−3.50	1.0
Oxalic acid	−0.107	−3.50	0.91	−0.016	−1.82	0.97
Citric acid	−0.069	−3.00	0.97	−0.013	−1.69	0.94

d_1 and d_2 are the decay coefficients for R caused by proton and ligand, respectively.

Table S2 Fitted parameters of the two-site dissolution model in the batch experiments

C_0	LMWOAs	$C[PO_4^{3-}]_{max1}$		k_1	$C[PO_4^{3-}]_{max2}$		k_2	R^2
(g L^{-1})		(%)	(mM)	(h^{-1})	(%)	(mM)	(h^{-1})	
0.2	Acetic acid	6.34	0.076	15.2	6.34	0.076	640	1.0
	Oxalic acid	16.0	0.191	6.04	6.50	0.078	6.04	1.0
	Citric acid	22.8	0.273	679	7.51	0.090	1.36	0.99
1	Acetic acid	2.62	0.157	14.9	0.500	0.030	5.84	0.99
	Oxalic acid	5.65	0.338	20.0	0.595	0.035	0.806	0.99
	Citric acid	8.17	0.488	35.0	1.09	0.065	0.194	0.99

$C[PO_4^{3-}]_{max1}$ and $C[PO_4^{3-}]_{max2}$ are the concentrations (mM) of total dissolved phosphate associated with site 1 and site 2, respectively; and k_1 and k_2 are the dissolution rate constants (h^{-1}) associated with site 1 site and 2, respectively.

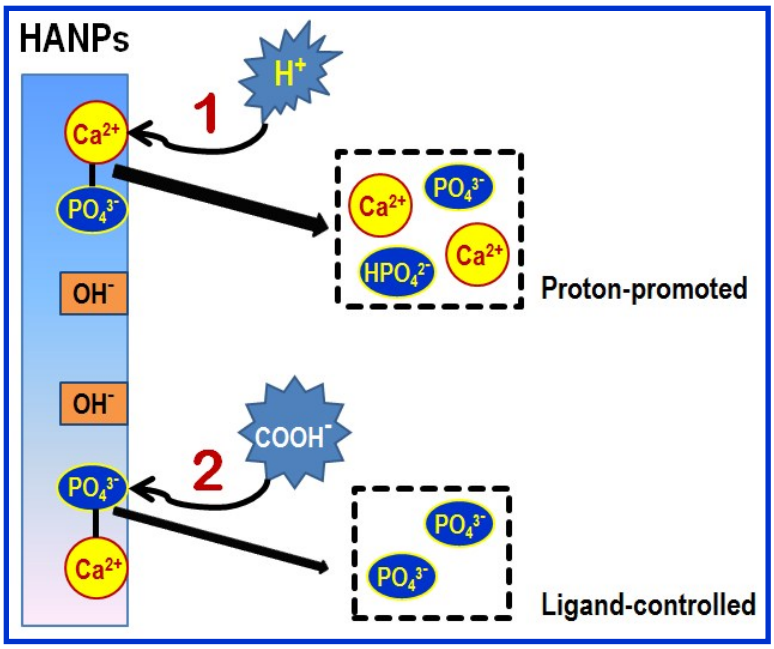

Fig. S1 Schematic illustration of HANPs dissolution mechanisms in the presence of LMWOA that includes proton (H^+) and ligand ($COOH^-$) functional groups. Proton-promoted dissolution (1) and ligand-controlled dissolution (2) are two major mechanisms controlling HANPs dissolution.

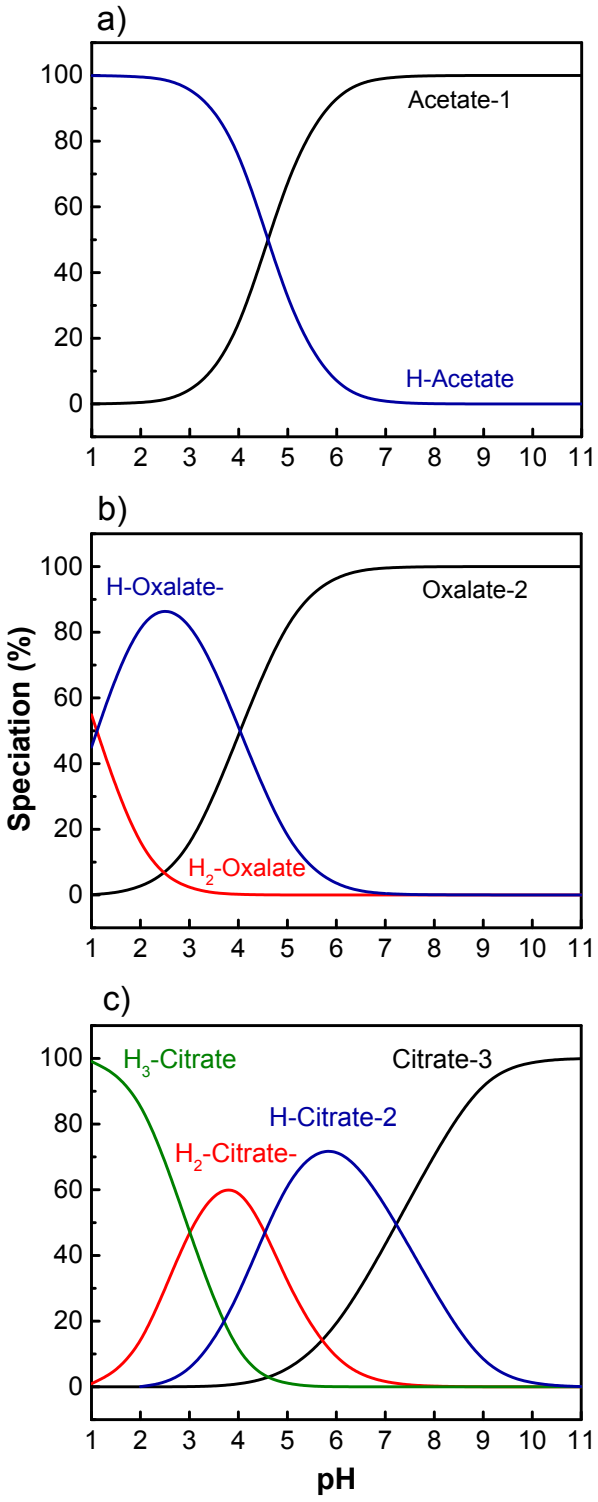

Fig. S2 Chemical speciation of 1 mM acetic acid (a), oxalic acid (b), and citric acid (c), respectively, versus pH calculated using the Visual MINTEQ 3.0 software.

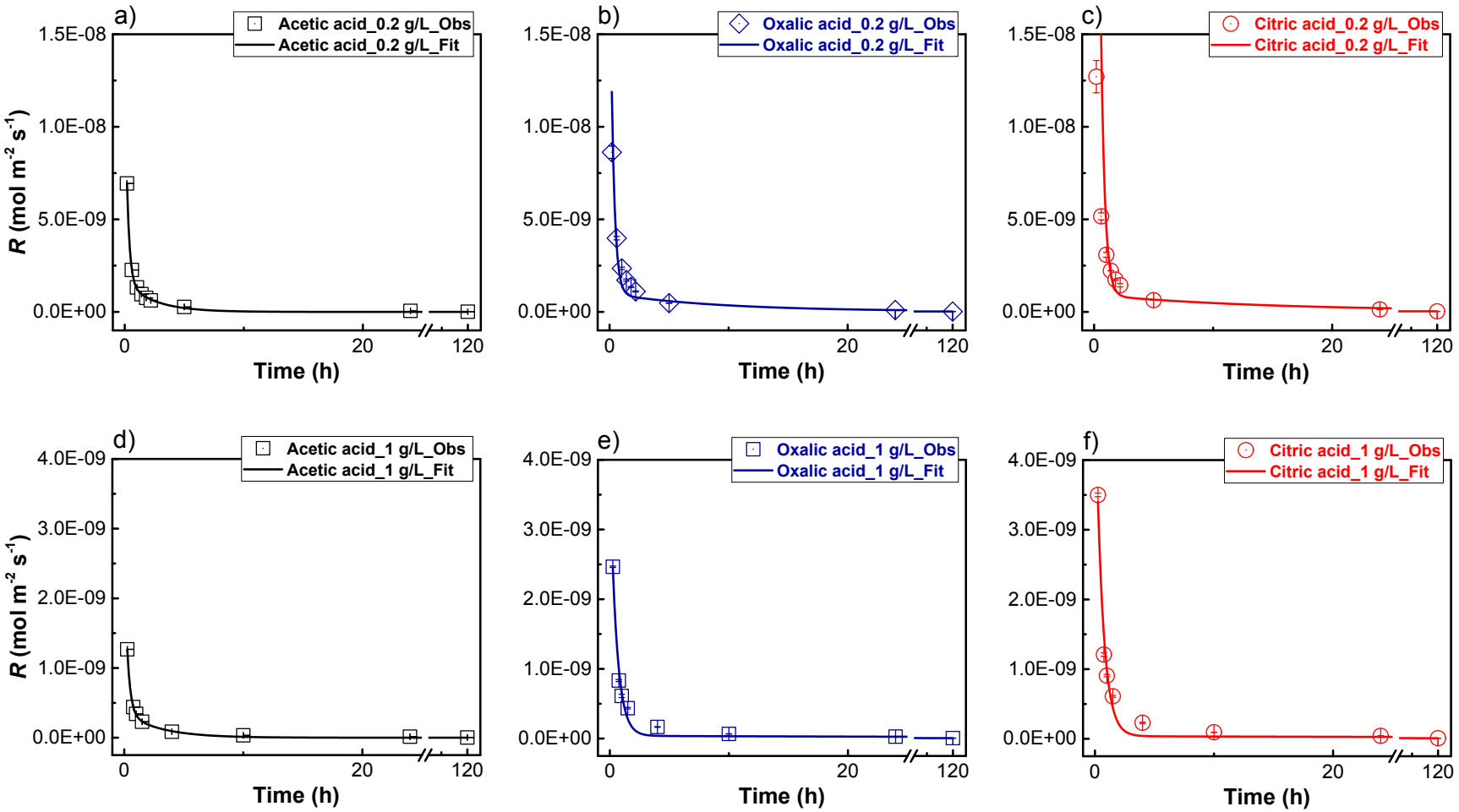

Fig. S3 Dissolution rate (R; mol m^{-2} s^{-1}) of HANPs versus time under different LMWOAs (1 mM acetic, oxalic, and citric acids, respectively) in batch experiments at initial HANPs concentrations (C_0) of 0.2 (a–c) and 1 g L^{-1} (d–f), respectively. Error bars represent the standard deviations in triplicate experiments. The data are fitted using the exponential decay function: $y = ae^{d_1 x} + be^{d_2 x}$; where d_1 and d_2 are the decay coefficients for R caused by proton and ligand, respectively; and a and b are constants.

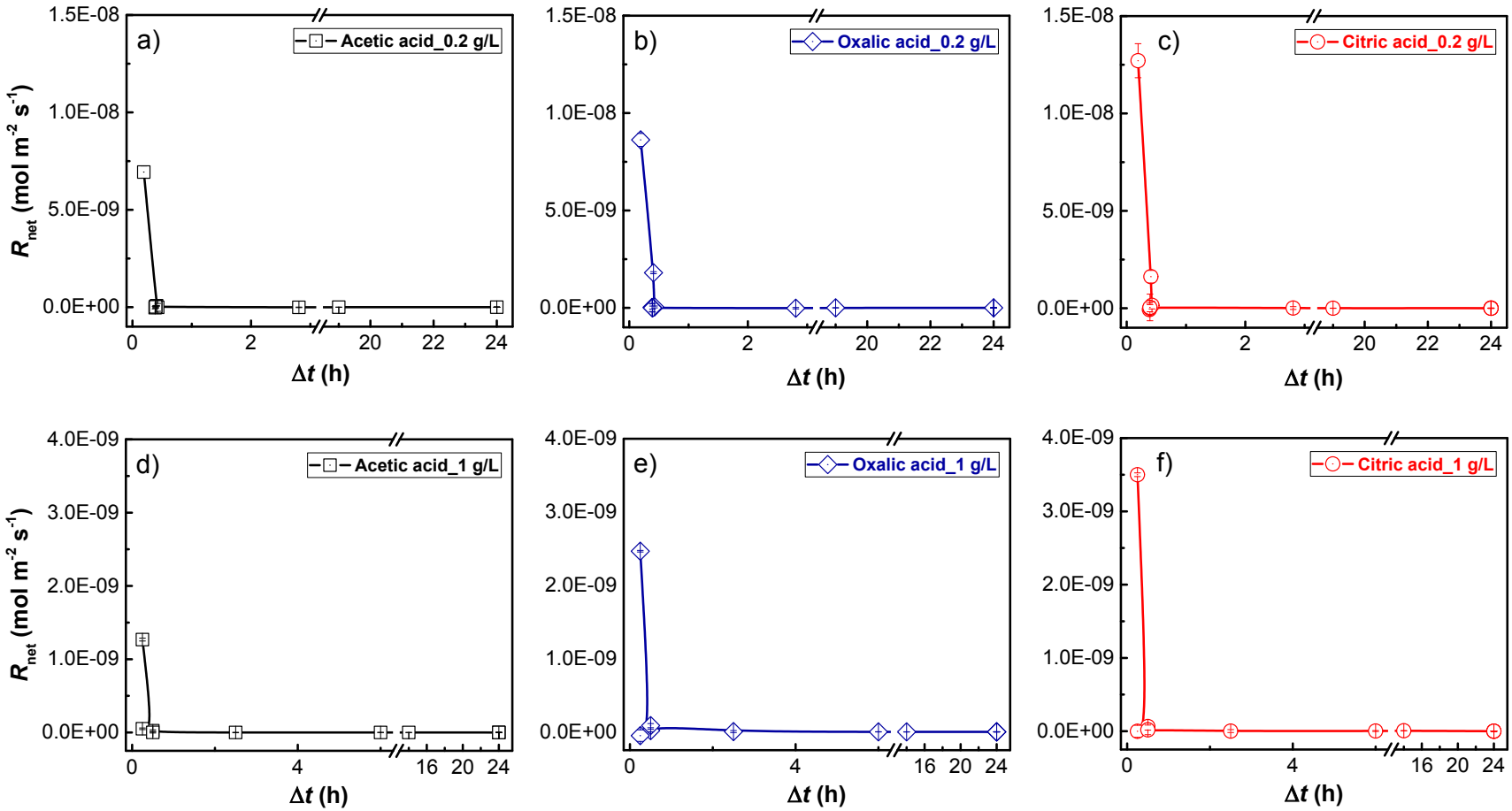

Fig. S4 Net dissolution rate (R_{net}; mol m^{-2} s^{-1}) of HANPs versus Δt under different LMWOAs (1 mM acetic, oxalic, and citric acids, respectively) in batch experiments at C_0=0.2 (a–c) and 1 g L^{-1} (d–f), respectively. Error bars represent the standard deviations in triplicate experiments. $R_{net} = \frac{dM}{S_i dt} = \frac{\Delta M_{21}}{S_i \Delta t_{21}}$, where ΔM_{21} is the mass consumption (mol) of HANPs from time t_1 to t_2 ($\Delta t_{21}=t_2-t_1$; $t_2>t_1$). Lines are just connections between data points.

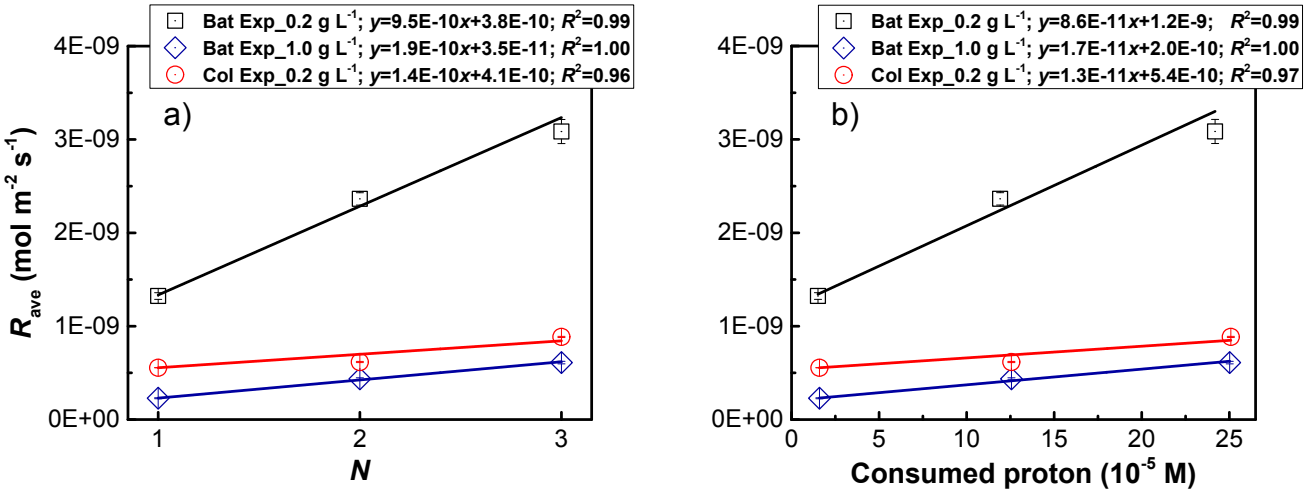

Fig. S5 Average dissolution rate (R_{ave}) of HANPs versus carboxyl group number (N; a) of LMWOAs (N=1, 2, and 3, respectively, for acetic, oxalic, and citric acids) and consumed amount of proton when the dissolution reaction reaches equilibrium (b) at C_0=0.2 and 1 g L^{-1} in batch experiments and C_0=0.2 g L^{-1} in column experiments. Error bars represent the standard deviations in triplicate experiments.

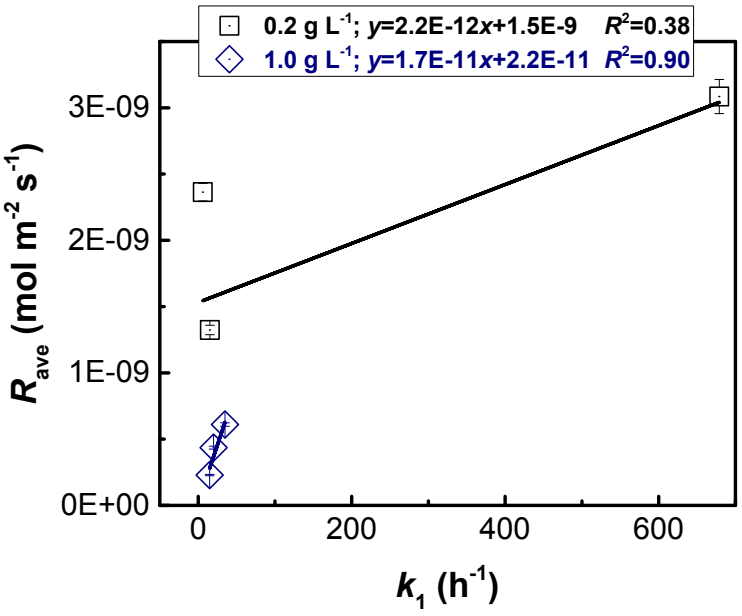

Fig. S6 Linear relationship between average dissolution rate (R_{ave}) and dissolution rate constant (k_1) on site 1 under different LMWOAs (1 mM acetic acid, oxalic acid, and citric acid, respectively) at C_0=0.2 and 1 g L^{-1} in batch experiments. Error bars represent the standard deviations in triplicate experiments.

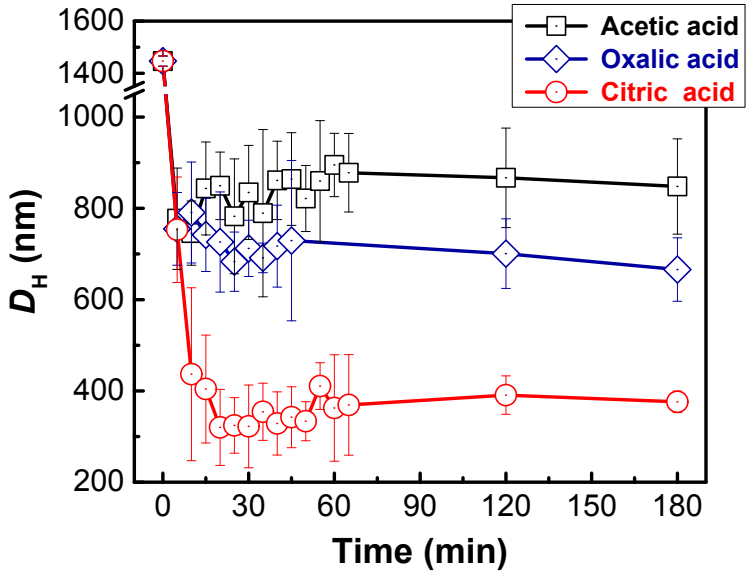

Fig. S7 Change in average hydrodynamic diameter (D_H) of HANPs versus time under 1 mM acetic acid, oxalic acid, and citric acid, respectively, at C_0=0.2 g L^{-1}. Error bars represent the standard deviations in triplicate experiments.

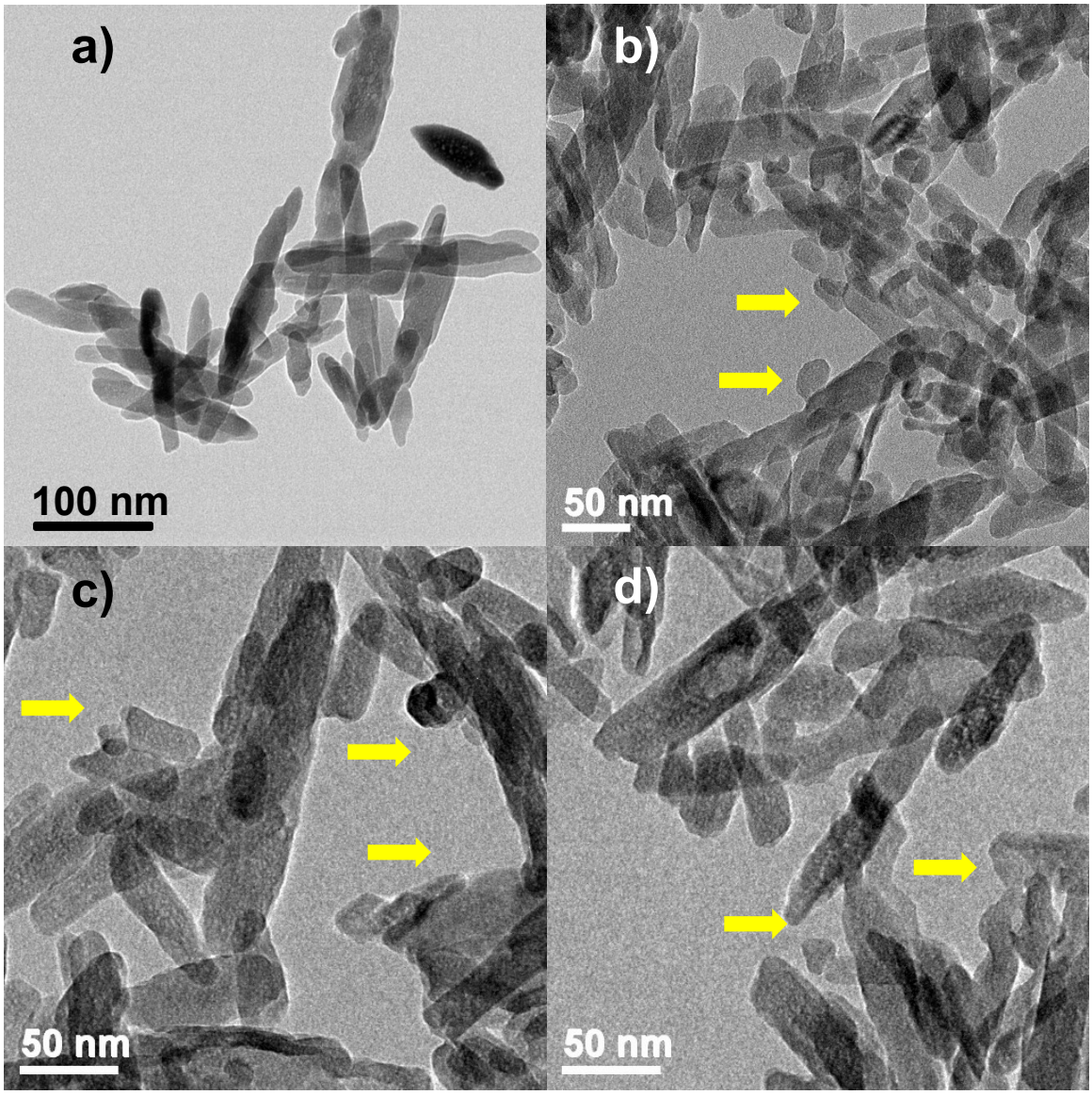

Fig. S8 TEM images of pristine (starting) HANPs (a) and partially dissolved HANPs (b−d) under 1 mM acetic acid at C_0=0.2 g L^{-1}.

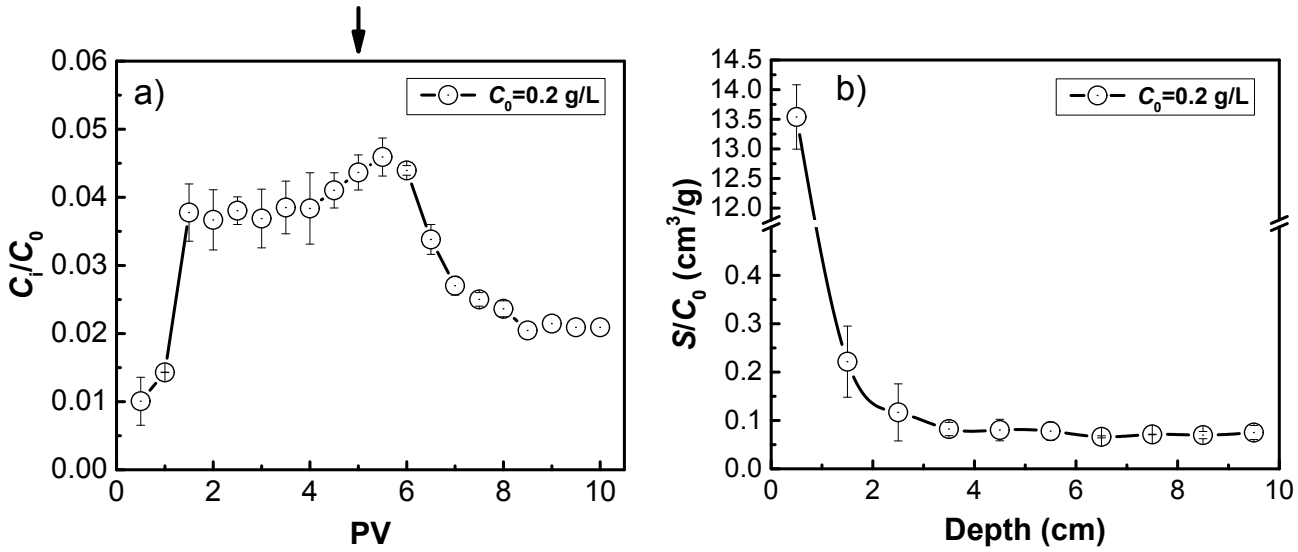

Fig. S9 Breakthrough curve (a) and retention profile (b) of HANPs at C_0=0.2 g L^{-1} in saturated quartz sand column. (a) Black arrow represents the duration of HANPs suspension injecting in the column. Error bars represent the standard deviations.

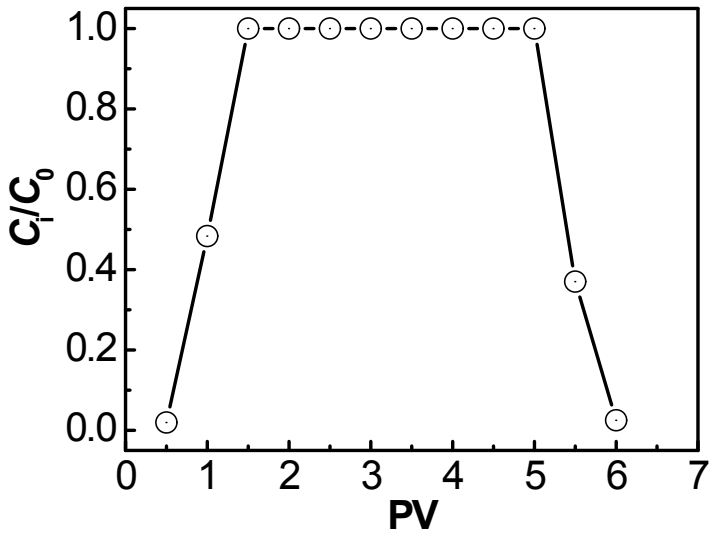

Fig. S10 Breakthrough curve of tracer (KNO_3) in saturated quartz sand column.

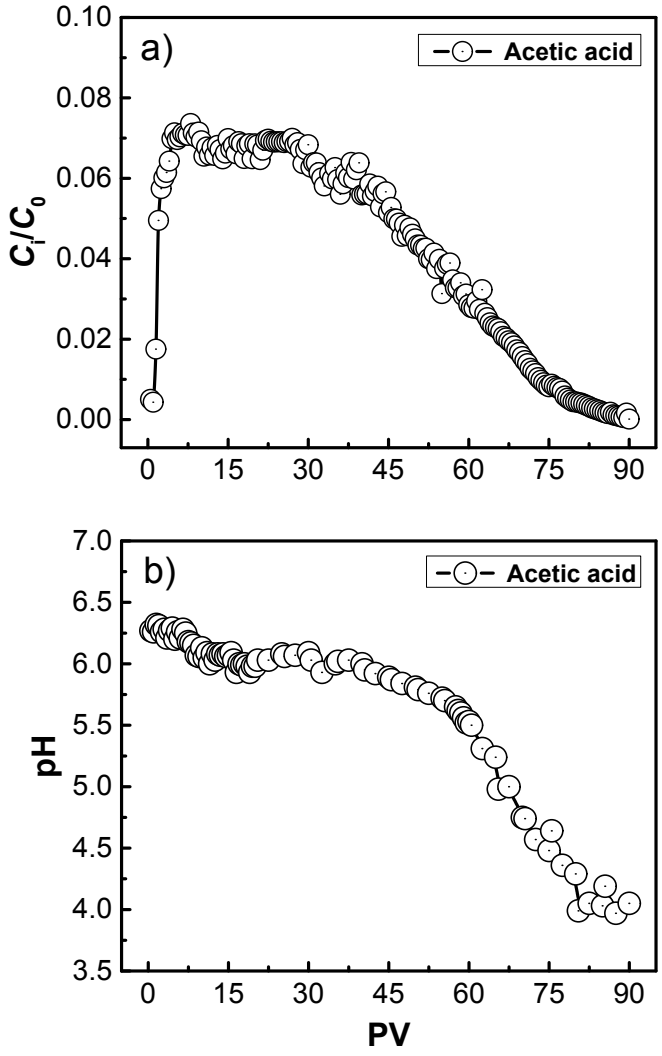

Fig. S11 Normalized effluent concentration (a) and effluent pH (b) versus PV when continuously injecting 90 PVs of 1 mM acetic acid to dissolve the HANPs retained in the column at C_0=1 g L^{-1}.

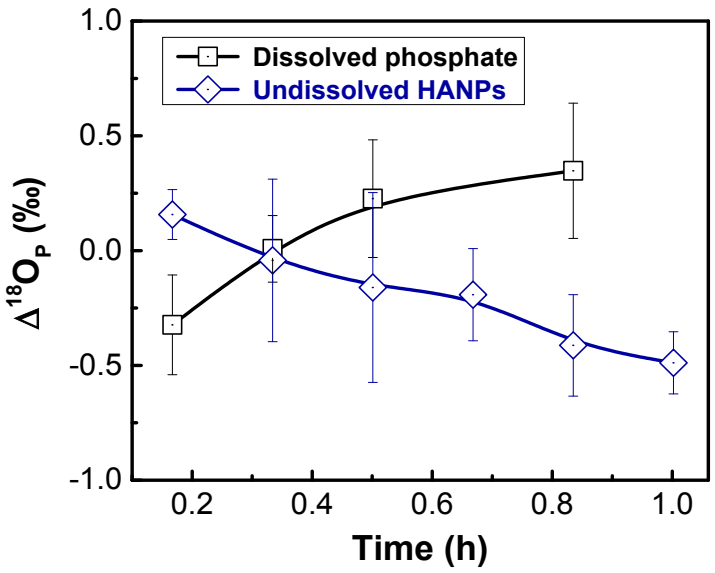

Fig. S12 Phosphate oxygen isotope ratios ($\delta^{18}O_P$) of dissolved phosphate and undissolved (particulate) HANPs under 1 mM oxalic acid over a short-time period (≤1 h) at C_0=1 g L^{-1}. Standard deviation is calculated from isotopic composition of phosphate from each sample. The $\Delta^{18}O_P$ describes phosphate oxygen isotope fractionation of dissolved phosphate (or undissolved HANPs) relative to the bulk (starting) HANPs ($\delta^{18}O_{P0}$), $\Delta^{18}O_P = \delta^{18}O_{P\text{-dissolved phosphate}} - \delta^{18}O_{P0}$ (or $\Delta^{18}O_P = \delta^{18}O_{P\text{-undissolved HANPs}} - \delta^{18}O_{P0}$).